Nucleic Acids Research, 2025, gkaf324
https://doi.org/10.1093/nar/gkaf324
RNA and RNA-protein complexes

The structure of the *Vibrio natriegens* 70S ribosome in complex with the proline-rich antimicrobial peptide Bac5(1–17)

Karoline Raulf[1,†], Timm O. Koller[1,†], Bertrand Beckert[1], Alexander Lepak[2], Martino Morici[1], Mario Mardirossian[3], Marco Scocchi[3], Gert Bange[2,*], Daniel N. Wilson[1,*]

[1]Institute for Biochemistry and Molecular Biology, University of Hamburg, Hamburg 20146, Germany
[2]Center for Synthetic Microbiology (SYNMIKRO) and Department of Chemistry, University of Marburg, Karl-von-Frisch-Strasse 14, 35043 Marburg, Germany
[3]Department of Life Sciences, University of Trieste, 34127 Trieste, Italy

[*]To whom correspondence should be addressed. Email: Daniel.wilson@uni-hamburg.de
Correspondence may also be addressed to Gert Bange. Email: bangeg@staff.uni-marburg.de
[†]The first two authors should be regarded as Joint First Authors.

Abstract

Proline-rich antimicrobial peptides (PrAMPs) are produced as part of the innate immune response of animals, insects, and plants. The well-characterized mammalian PrAMP bactenecin-5 (Bac5) has been shown to help fight bacterial infection by binding to the bacterial ribosome and inhibiting protein synthesis. In the absence of Bac5-ribosome structures, the binding mode of Bac5 and exact mechanism of action has remained unclear. Here, we present a cryo-electron microscopy structure of Bac5 in complex with the 70S ribosome from the Gram-negative marine bacterium *Vibrio natriegens*. The structure shows that, despite sequence similarity to Bac7 and other type I PrAMPs, Bac5 displays a completely distinct mode of interaction with the ribosomal exit tunnel. Bac5 overlaps with the binding site of both A- and P-site transfer RNAs bound at the peptidyltransferase center, suggesting that this type I PrAMP can interfere with late stages of translation initiation as well as early stages of elongation. Collectively, our study presents a ribosome structure from *V. natriegens*, a fast-growing bacterium that has interesting biotechnological and synthetic biology applications, as well as providing additional insights into the diverse binding modes that type I PrAMPs can utilize to inhibit protein synthesis.

Graphical abstract

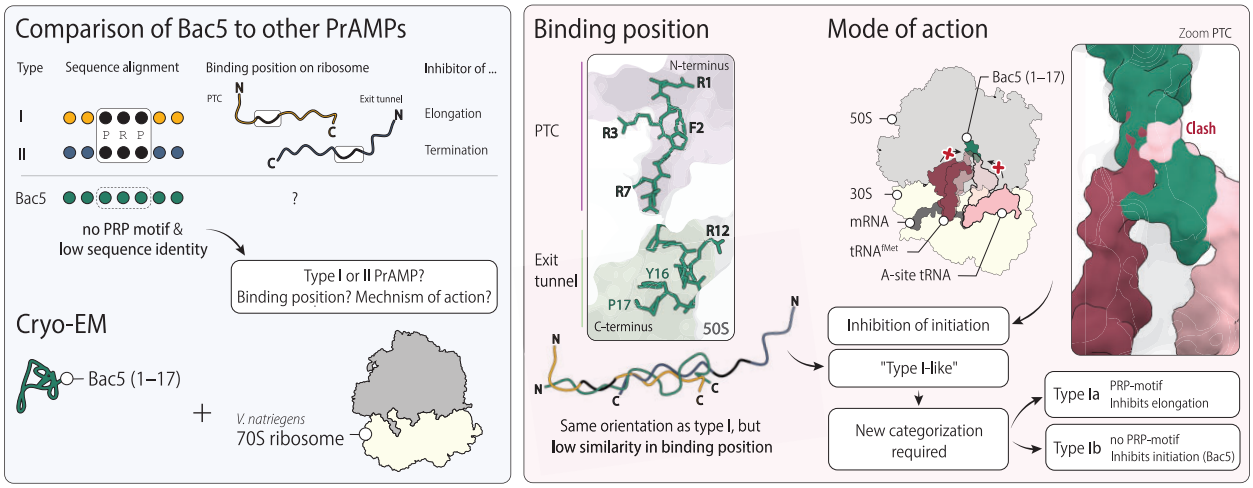

Introduction

PrAMPs comprise part of the innate immune system to combat bacterial infection and have been identified in many insects and some mammals, specifically ruminants and cetaceans, including e.g. sheep, cows, goats, dolphins, and whales [1–5] (Fig. 1A). Unlike most AMPs that damage the bacterial

Received: December 13, 2024. **Revised:** March 27, 2025. **Editorial Decision:** April 5, 2025. **Accepted:** April 14, 2025

A

Name	Organism	Sequence	Length	Type	
Apidaecin 1b	*Apis mellifera*	GNNRPVYIPQ**PRP**PHPRL	18 aa	II	Arthropods
Apidaecin 137 (Api137)	Synthetic	Gu–ONNRPVYI**PRP**R**P**PHPRL	18 aa	II	
Drosocin (Dro)	*Drosophila melanogaster*	GKPRPYS**PRP**T*SHPRPIRV	19 aa	II	
Oncocin	*Oncopeltus fasciatus*	VDKPPYL**PRP**P**P**PRRIYNNR–OH	20 aa	I	
Oncocin 112 (Onc112)	Synthetic	VDKPPYL**PRP**R**P**PRrIYNr–NH_2	19 aa	I	
Pyrrhocoricin (Pyr)	*Pyrrhocoris apterus*	VDKGSYL**PRP**T**P**PRPIYNRN	20 aa	I	
Metalnikowin-1(Met-1)	*Palomena prasina*	VDKPDYR**PRP**R**P**PNM	15 aa	I	
Tur1A	*Tursiops truncatus*	RRIRFRPPYL**PRP**GRRPRFPPPFPIPRIPRIP	32 aa	I	Mammals
Bactenecin 7 (Bac7)	*Bos taurus*	RRIRP**RPPRL**PRP**R**PRRPLPFPRPGPRPIPRP..	60 aa	I	
Bactenecin 5 (Bac5)	*Bos taurus*	RFRPPIRRPPIRPPFYPPFRPPIRPPIFPPIR..	43 aa	?	

consensus site

Bold: PRP-P motif Gu: N, N, N′, N′-tetramethylguanidino O: L-ornithin r: D-arginine *: O-glycosylation

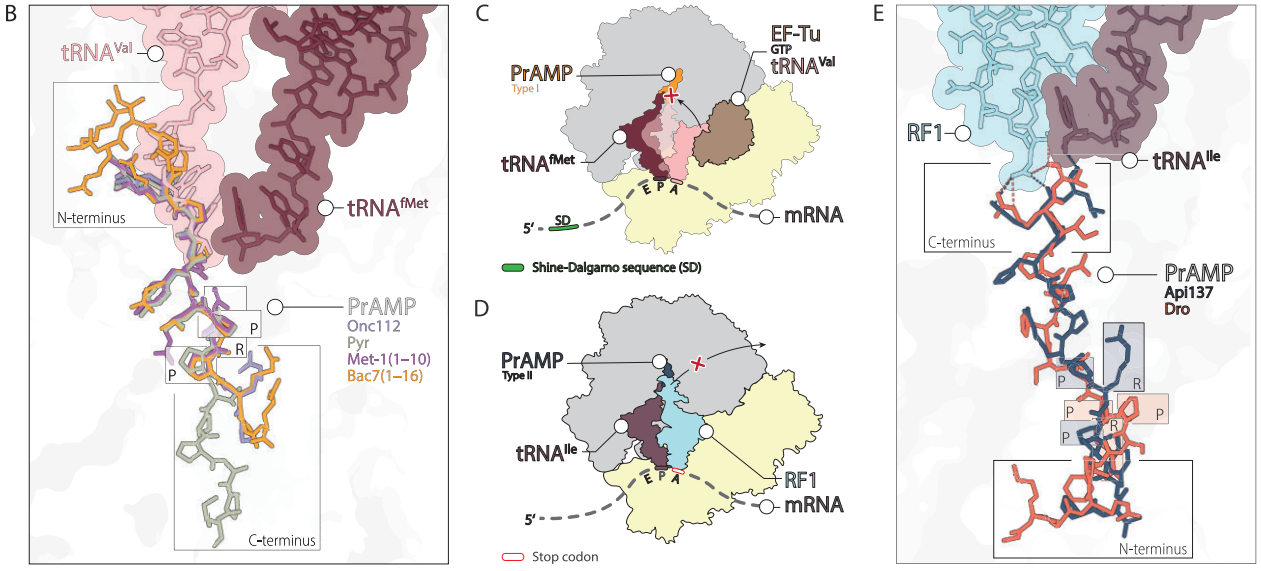

Figure 1. Summary of the origin, nature and mode of action of the most commonly known PrAMPs. (**A**) Sequence alignment of naturally occurring and synthetically produced PrAMPs of types I and II. The consensus sequence is indicated by a dashed box, and the conserved PRP motif is highlighted in bold. (**B**) Superimposition of the type I peptides Onc112 [6], Pyr [8], Met-1 (1–10) [8], and Bac7 (1–16) [8]. The alignments are based on the ribosomal RNA (rRNA) structure of the respective model organism. Additionally, the alignment of the initiator tRNA in the P-site (fMet) and the A-site tRNA (Val) [36] illustrates the mechanism of action of type I PrAMPs. This mode of action is further visualized in panel (**C**) (Elongating ribosome with EF-Tu*GTP). (**D**) Illustration of the mode of action of type II PrAMPs (RF1) and P-site $tRNA^{Ile}$. (**E**) Superimposition of type II PrAMPs Api137 [12] and Dro [15]. The alignment with RF1 and the P-site $tRNA^{Ile}$ highlights the previously described mechanism. This figure was adapted from reference [2].

membrane, PrAMPs pass through the membrane and bind to the ribosome to inhibit translation [2, 3]. Structures of PrAMP-ribosome complexes reveal that these peptides exert their inhibitory function by binding within the nascent polypeptide exit tunnel (NPET) located on the large 50S ribosomal subunit [2, 3]. To date, PrAMPs appear to fall into two main categories, type I and type II [2, 3]. Type I PrAMPs bind within the NPET with the N-terminus located in a position that overlaps with the 3′-end of an incoming A-site transfer RNA (tRNA) (Fig. 1B) and thus their mechanism of action is to prevent peptide bond formation by blocking the accommodation of the A-site tRNA on the large subunit (Fig. 1C). Structurally well-characterized type I PrAMPs include the insect PrAMPs oncocin, pyrrhocoricin and metalnikowin-1, the mammalian Tur1A, bactenecin-7 fragments, and more recently, rumicidin-2 [5–11]. By contrast, type II PrAMPs bind within the NPET with the C-terminus located at the peptidyltransferase center (PTC) where they establish interactions with the termination release factors (RFs) (Fig. 1D and E). By stabilizing RFs on the ribosome (Fig. 1E), type II PrAMPs not only interfere with translation in *cis*, but also cause a global reduction in translation termination due to the sequestration of RFs [12]. Structurally well-characterized type II PrAMPs include the insect PrAMPs apidaecin from wasps and bees, as well as drosocin from fruit flies [12–16].

Despite the intensive structural characterization of diverse type I and II PrAMPs, a structure of the mammalian bactenecin-5 (Bac5) PrAMP has so far been lacking. The native Bac5 is 43 amino acids in length, however, shorter N-terminal fragments of Bac5 retain antimicrobial activity [17–19]. N-terminal truncation of Bac5 is not well-tolerated, with the removal of only four amino acids from the N-terminus leading to complete loss of antimicrobial activity for the shorter fragment Bac5(1–25) [11, 19, 20]. The shortest active fragment, Bac5(1–17), was used to generate a library of derivatives with 1–5 substitutions, leading to the discovery of five Bac5(1–17) derivatives with increased arginine and tryptophan content. These derivatives exhibited improved antimicrobial activity, while retaining low cytotoxicity toward eukaryotic cells [19]. Like other PrAMPs, the SbmA trans-

porter plays a critical role in the cellular uptake of Bac5 in *Escherichia coli* [17, 18], however, some of the new Bac5 derivatives displayed a moderate membrane destabilizing activity that conferred a broader spectrum of activity, even against bacterial species lacking SbmA [19]. Biochemical assays indicate that the shorter N-terminal fragments of Bac5 trap ribosomes at the initiation codon of the messenger RNA (mRNA) [17], consistent with the type I mechanism of action described for the related PrAMP, Bac7 [8, 9]. Although Bac5 shares a high proline and arginine content with Bac7, the low sequence identity (Fig. 1A) makes it hard to predict how Bac5 will interact with the ribosome. Therefore, a structure of Bac5 on the ribosome will be essential to not only decipher its mechanism of action, but also to further develop this PrAMP as a novel antimicrobial agent.

Rather than determining a structure of Bac5 in complex with ribosomes from an organism, such as *E. coli*, for which ribosomes structures already exist, we set out to determine a structure of Bac5 in complex with ribosomes from an organism where the ribosome structure does not exist. We chose for this the ribosomes from the fast-growing Gram-negative marine bacterium *Vibrio natriegens* [21], which was originally discovered in the late 1950's [22]. While *E. coli* is one of the most frequently used bacterial systems for molecular biology techniques due to its rapid growth in rich media, with a doubling rate of between 20 and 30 min [23], there has been growing interest in *V. natriegens* as an alternative system due to its rapid growth rate, with a doubling time of 10 min, thus, exceeding *E. coli* by a factor of 2–3-fold [24, 25]. To date, most standard molecular biology methods have already been adapted for use with *V. natriegens*, such as cloning, transformation, and genome editing [23, 26, 27]. A great example of the major benefits of using *V. natriegens* instead of *E. coli* is a study where colonies could be observed on plates 6 h after transformation [23]. A subsequent DNA isolation could then be completed within <3 h, by-passing the overnight incubation that is necessary when using *E. coli* cells [23]. The use of *V. natriegens* could therefore lead to significant time savings during day-to-day laboratory usage. Despite the interest in *V. natriegens* for development as a molecular biology tool and use as a protein expression system, the ribosomes of *V. natriegens* have so far not been structurally characterized.

Here, we report a cryo-EM structure of the *V. natriegens* 70S ribosome in complex with Bac5(1–17) at 2.8 Å resolution. Although *V. natriegens* is not naturally sensitive to PrAMPs due to the lack of SbmA transporter, we could demonstrate that overexpression of SbmA in *V. natriegens* makes the strain susceptible to both Bac5 and Bac7. Moreover, we could validate the inhibitory activity of Bac5 on *V. natriegens* ribosomes using a hybrid *in vitro* translation system. The structure of the Bac5-70S ribosome complex reveals that the binding mode and details of interaction of Bac5 are completely distinct from Bac7, consistent with the differences in sequence between these two PrAMPs. Nevertheless, like Bac7, Bac5 also binds within the NPET with the N-terminus located in a position that overlaps with the CCA-end of an incoming A-site tRNA, which is consistent with the biochemistry suggesting that the mechanism of action of Bac5 is to prevent peptide bond formation by blocking the accommodation of the A-site tRNA on the large subunit [17]. Collectively, our study reveals not only the versatility of *V. natriegens* as molecular biology tool, but also provides insight into the mechanism action by which the PrAMP Bac5 binds to ribosomes to inhibit protein synthesis.

Materials and methods

Strains and plasmids

Bac5(1–17) and Bac7(1–16) were synthesized by NovoPro (China), whereas spectinomycin was purchased from Sigma. The *E. coli* Δ*sbmA* strain was obtained from the Keio collection [28]. The *V. natriegens* strain ATCC14048, was acquired through the German Collection of Microorganisms and Cell Cultures GmbH (DSMZ). The *E. coli sbmA* gene was cloned into pAL0155_ColE1 plasmid created from the Marburg collection, a cloning toolbox optimized for *V. natriegens*. The plasmids contained the high copy ColE1 (pAL0155) ori, a tetracycline-inducible promotor, the B0034 ribosome binding site, the B1003 terminator, and a chloramphenicol resistance cassette [29]. The details of each part are published elsewhere [29] and the plasmid sequences are presented in the Supplementary Table S1. For SbmA expression, a C-terminal His-tagged version of the *sbmA* gene was cloned into the plasmid pAL0155_ColE1_sfGFP, while the control plasmid contained sfGFP (pAL0167_ColE1_sfGFP). Plasmids pAL0155_ColE1_SbmA and pAL0167_ColE1_sfGFP were transformed into *V. natriegens* strain ATCC14048.

Bacterial growth assay

To test the effect of Bac5 and Bac7 on the growth of *V. natriegens* and *E. coli* cells, a growth inhibition assay was performed. For this purpose, four different concentrations (1, 10, 25, and 100 μM) of each peptide were titrated; the negative control for inhibition contained no PrAMP and the positive control for inhibition contained 25 μM erythromycin. Any inhibiting effect was evaluated monitoring the optical density (OD) at 600 nm (OD_{600}) over a 15-h period using the infinite 200Pro microplate reader (TECAN). All measurements were performed in a 96-well microplate, each with a total volume of 150 μl. The wells in the outer area of the plate were excluded from the experimentation and filled only with 300 μl of sterilized MiliQ water to reduce evaporation effects during the measurements. For the assay, precultures of the bacteria to be tested (*V. natriegens*: wt; *E. coli* BW25113: wt, Δ*sbmA*) were first prepared and incubated for 10 h at 37°C and 120 rpm. In the case of *V. natriegens*, the growth medium chosen was Brain Heart Infusion (BHI) and for *E. coli* cells Luria Broth (LB) medium. Based on the OD_{600} values of these cultures, the volumes of each test component were then calculated in order to have all the bacterial cultures with an $OD_{600} = 0.05$ at the starting point. In the case of *V. natriegens* cells, an additional 1 μg/ml chloramphenicol and 0.22 μg/ml tetracycline (inducing SbmA expression) were added. Cultivation of the *E. coli* Δ*sbmA* strain required the addition of 25 μg/ml kanamycin.

Vibrio natriegens ribosome preparation

Purification of reassociated *V. natriegens* 70S ribosomes was performed as described previously for reassociated *E. coli* 70S ribosomes [30]. Briefly, ribosomes were first isolated from the cell lysates by centrifugation using 30% sucrose cushion, run at 30 000 rpm (in a Ti45 rotor) at 4°C for 17.5 h. The pelleted crude ribosomes were then resuspended in $H_{25}K_{100}M_6$ and 200 $Absorbance_{260}$ (A_{260}) units were loaded onto a linear sucrose gradient (5%–30%). Gradients were run at 30 000 rpm

(in a SW32 rotor) at 4°C for 3 h 45 min and the 70S peak fractions were collected. These purified 70S ribosomes were then dissociated into subunits by lowering the Mg^{2+} concentration (resuspension in $H_{20}M_1N_{200}SH_4$ and incubated at 4°C for 1 h). The dissociated subunits were subsequently loaded onto another sucrose gradient (5%–30%) and run at 16 000 rpm (in a SW32 rotor) at 4°C for 16 h. The fractions corresponding to the 30S and 50S subunits were then collected separately, repelleted and reassociated to form 70S ribosomes by resuspension in a buffer containing $H_{20}M_{20}K_{30}$ at 37°C for 40 min in a molar ratio of 30S:50S of 1:1.2. A total of 20 A_{260} of the reassociated 70S ribosomes were then loaded on a sucrose gradient (5%–30%) and gradients were run at 35 000 rpm (in a SW40 rotor) at 4°C for 3 h and the reassociated 70S ribosomes were repelleted and resuspended in buffer containing $H_{20}M_{10}K_{30}$.

For the *in vitro* translation assays, crude ribosomes were purified as follows: subsequently to inoculation, *V. natriegens* were grown at 37°C in BHI + 2.5% (w/v) NaCl until mid-log phase (OD_{600} = 0.5–0.7), and then harvested by centrifugation (rotor JLA 8.1000, 8000 × *g*, 20 min at room temperature) and the pellet was resuspended in minimal volume of Buffer A [50 mM Hepes–KOH, pH = 7.2 (4°C), 500 mM KOAc, 10 mM MgOAc, 0.1% (w/v) n-dodecyl-β-D-maltosid (DDM), 1 mM dithiothreitol (DTT)]. Cells were pelleted again as before and resuspended in 20 ml (0.15 ml/A_{600}) of Buffer B [Buffer A + 5 U/ml murine RNase inhibitor (NEB) + 1 tablet/10 ml of cOmplete™ ethylenediaminetetraacetic acid-free Protease Inhibitor Cocktail (Merck)], and subsequently homogenized by french press (3 × 18 000 psi cycles). Such lysate was cleared to remove the cell debris (rotor JA 25.50, 15 000 × *g*, 20 min, 4°C) and then layered on a sucrose cushion [50 mM Hepes–KOH, pH = 7.2 (4°C), 500 mM KOAc, 10 mM MgOAc, 1 mM DTT, 25% (w/v) sucrose], to undergo an overnight (>16 h) ultracentrifugation (rotor Ti70, 30 000 rpm, 4°C). The pellet was resuspended in minimal volume (500 µl) of Buffer B and layered on a second sucrose cushion [50 mM Hepes–KOH, pH = 7.2 (4°C), 500 mM KOAc, 10 mM MgOAc, 0.1% (w/v) DDM, 1 mM DTT, 25% (w/v) sucrose], to undergo ultracentrifugation (rotor TLA120, 80 000 × *g*, 3 h, 4°C). The pellet was resuspended in a minimal volume (30 µl) of Buffer C [50 mM Hepes–KOH, pH = 7.4 (4°C), 100 mM KOAc, 10 mM MgOAc, 80 mM NH_4Cl, 0.01% (w/v) DDM, 1 mM DTT] and the ribosomes quantified by nanodrop (A_{260}/ml). All the buffers described were filtered (molecular weight cut-off = 0.2 µm).

In vitro translation assay

The *in vitro* translation assay was carried out similarly as described previously [15], using the *E. coli* PURExpress system Δ ribosome (New England Biolabs, NEB). Briefly, 1 µl of crude *V. natriegens* ribosomes in Buffer C isolated as described before, corresponding to 15 pmol of 70S, was used instead of *E. coli* ribosomes from the kit in 5 µl of PURExpress reaction mix, to which 1 µl of antibiotic solution was added. Each reaction contained 16 ng/µl of mRNA encoding the Fluc, which was *in vitro* transcribed from a pIVEX-2.3MCS vector containing the Fluc gene using T7 polymerase (Thermo Fisher Scientific). The reaction mix without the mRNA was first pre-incubated for 2 min at 32°C while shaking (600 rpm), then, subsequently to mRNA addition, the reaction mix is incubated for 30 min at 32°C while shaking (600 rpm). Reactions were stopped with 5 µl of kanamycin (50 µg/ml) and transferred into a 96-well microplate (Greiner Lumitrac, non-binding, white, chimney). Next, 40 µl of luciferase assay substrate solution (Promega, E1501) was added, and luminescence was measured using a plate reader (Tecan Infinite 200 PRO). Nuclease-free water was added instead of antibiotic as a control. Absolute luminescence values were normalized using reactions without antibiotic. All assays were done as triplicates with individually prepared reaction mix.

Preparation of cryo-EM sample, grids and data collection

The *V. natriegens* reassociated 70S ribosomes were incubated with 100 µM Spectinomycin and 100 µM Bac5 at room temperature for 15 min, and subsequently 3.5 µl of the complex (8 OD_{260}/ml) was applied to grids (Quantifoil, Cu, 300 mesh, R3/3 with 3 nm carbon) which had been freshly glow discharged using a GloQube (Quorum Technologies) in negative charge mode at 25 mA for 90 s. Sample vitrification was performed using ethane/propane mix in a Vitrobot Mark IV (Thermo Scientific), with the chamber set to 4°C and 100% relative humidity, and blotting was performed for 3 s with no drain or wait time. The grids were subsequently mounted into the Autogrid cartridges and loaded onto the Talos Arctica (Thermo Fischer Scientific) TEM for screening. Grids were stored in liquid nitrogen until high resolution data collection. High resolution data was collected on a Titan Krios microscope aligned for fringe-free imaging and equipped with Falcon 2 (FEI) direct electron detector. The camera was operated in correlated double sampling mode and the data was collected at the pixel size of 1.061 Å/px. The microscope condenser system was set to produce 40 e/Å^{2}s electron flux on the specimen and the data from 1.8 s exposure were stored into 40 frames. The data from 3 × 3 neighboring holes were collected using beam/image shifting while compensating for the additional coma aberration. The data was collected with the nominal defocus range of −0.7 to −1.2 µm. A total number of 3 878 movies were collected.

Single-particle reconstruction of *V. natriegens* 70S ribosome complex

RELION v4.0.1 [31] was used for processing, unless otherwise specified. For motion correction, RELION's implementation of MotionCor2 with 4 × 4 patches and for initial Contrast Transfer Function (CTF) estimation CTFFIND v4.1.14 [32] was employed. From 3878 micrographs, ribosome-like particles were picked using crYOLO v1.8.04b47 with a general model [33]. A total of 405 140 ribosome-like particles were selected after 2D classification and extracted at 3x decimated pixel size (3.183 Å/pixel) (Supplementary Fig. S1A–C). An initial 3D refinement was done using a *E. coli* 70S reference map (EMD-12573) [34]. Particles were 3D classified for 100 iterations, resulting in six classes, of which three 70S classes with differing degrees of intersubunit rotation (Supplementary Fig. S1D) were combined and either processed using a 70S mask (Supplementary Fig. S1E), 50S mask (Supplementary Fig. S1F) or 30S mask (Supplementary Fig. S1G). All resulting classes were 3D refined (with a solvent mask), CTF refined (fourth order aberration, anisotropic magnification and per-particle defocus value estimation), Bayesian polished, again CTF refined and after a final 3D refinement yielded a final average resolution of 2.8 Å (at $FSC_{0.143}$)

for the post-processed masked reconstruction of the 70S (Supplementary Fig. S2A), 2.7 Å (at $FSC_{0.143}$) for the post-processed masked reconstruction of the 50S (Supplementary Fig. S2B), and 2.8 Å (at $FSC_{0.143}$) for the post-processed masked reconstruction of the 30S (Supplementary Fig. S2C). To estimate local resolution values Bsoft [35] was used on the half-maps of the final reconstructions (blocres -sampling 1.061 -maxres -boc 20 -cutoff 0.143 -verbose 1 -origin 0,0,0 -Mask half_map1 half_map 2) (Supplementary Fig. S2D-I).

Molecular modelling of the *V. natriegens* 70S ribosome complex

The molecular models of the 30S and 50S ribosomal subunits were based on the *E. coli* 70S ribosome (PDB ID 7K00) [36] due to homology of the overall model. Starting models were rigid body fitted using ChimeraX v1.6.1 [37] and 23S and 16S ribosomal RNA sequences were manually adjusted using Coot 0.9.8.92 [38] from the CCP4 software suite version 8.0.017 [39]. Ribosomal proteins were generated using Alphafold 2 [40, 41] within ChimeraX v1.6.1 [37], rigid body fitted and real space refined with Coot 0.9.8.92 [38]. The molecular model of bactenecin-5 was created de-novo in Coot 0.9.8.92 [38] and real-space refined. Restraints for the molecular model of spectinomycin (PDB ID 8CA7) [42] were created using aceDRG [43] and modelled and real-space refined in Coot 0.9.8.92 [38]. Final refinements were done in REFMAC 5 [44] using Servalcat v.0.4.28 [45]. The molecular models were validated using Phenix comprehensive cryo-EM validation in Phenix 1.20.1–4487 [46] (Supplementary Table S2).

Figures

UCSF ChimeraX 1.8 [37] was used to isolate density, align molecular models and visualize density images and structural superpositions. Figures were assembled with Adobe Illustrator 2024 (latest development release, regularly updated). Microsoft Excel and GraphPad Prism were used for data analysis and graphic representation of the *in vivo* growth assay and *in vitro* translation assay results.

Results

Bac5(1–17) inhibits *V. natriegens* expressing SbmA

One of the main goals of the study was to determine a structure of the *V. natriegens* 70S ribosome, but rather than determining a structure of a vacant 70S ribosome, we rationalized that it would be more insightful to visualize the ribosome in complex with a structurally uncharacterized PrAMP. Phylogenetic analysis indicates that *V. natriegens* 70S ribosome is likely to be closely related to the *E. coli* 70S ribosome, since both are Gram-negative γ-proteobacteria. Nevertheless, unlike *E. coli*, most *Vibrio* species, including *V. natriegens*, do not appear to contain the SbmA transporter that plays an important role for the uptake of PrAMPs [2, 3, 47]. To assess whether *V. natriegens* is sensitive to PrAMPs, we grew *V. natriegens* in the presence of increasing concentrations of Bac5(1–17), Bac7(1–16), as well as an inhibitory concentration (25 μM) of the macrolide erythromycin (Fig. 2A). As additional controls, we also performed the same experiment with Bac5(1–17) using the *E. coli* strain BW251113 that contains SbmA, as well as an *E. coli* BW251113 Δ*sbmA* deletion strain (Fig. 2B). As expected, increasing concentrations of Bac5(1–17) led to a dose-dependent inhibition of the growth of *E. coli* strain BW251113, but not in the case of the *E. coli* BW251113 Δ*sbmA* that lacks SbmA (Fig. 2B), consistent with previous reports that SbmA is the major transporter to uptake of Bac5(1–17) [19]. By contrast, Bac5(1–17) and Bac7(1–16) did not inhibit growth of *V. natriegens*, even at the highest concentration tested of 100 μM, whereas complete inhibition was observed with the control antibiotic erythromycin (Fig. 2A). Previous studies have demonstrated that *Pseudomonas aeruginosa* strains that also lack SbmA are less sensitive to PrAMPs, such as Bac7(1–35), but that they can be rendered fully sensitive to the PrAMP by heterologous expression of the *E. coli* SbmA protein [48]. To assess whether such an approach would also work for *V. natriegens*, we cloned the *E. coli sbmA* gene into a suitable plasmid for expression in *V. natriegens* (see the 'Materials and methods' section). As seen in Fig. 2C, *V. natriegens* strains expressing SbmA, but not those with the vacant plasmid control, became sensitive to both Bac5(1–17) as well as Bac7(1–16), suggesting that the insensitivity of *V. natriegens* to PrAMPs, such as Bac5(1–17) and Bac7(1–16), is due to lack of uptake and not because these PrAMPs cannot interact with their intracellular target, the ribosome. To demonstrate that Bac5(1–17) can directly interact with *V. natriegens* ribosomes, we investigated whether Bac5(1–17) can inhibit protein synthesis on *V. natriegens* ribosomes *in vitro*. It has been previously reported that the Gram-positive *Bacillus subtilis* 70S ribosomes can function together with *E. coli* translation factors in a hybrid version of the PURExpress translation system [49], therefore, we rationalized Gram-negative *V. natriegens* ribosomes may also function in such a hybrid assay. To do this, we generated reassociated *V. natriegens* 70S ribosomes (see the 'Materials and methods' section), which we could demonstrate were active in producing the firefly luciferase reporter protein, as evident from the luminescence generated in the presence of reporter mRNA, but absence of PrAMP (Fig. 2D). Importantly, we observed a dose-dependent decrease in luminescence with increasing concentration of Bac5(1–17), yielding an IC_{50} of 75 μM. Although this IC_{50} value is higher than that observed using the *E. coli* system [19], it nevertheless suggests that Bac5(1–17) can bind to and inhibit the *V. natriegens* ribosome and that Bac5(1–17) could be used to generate *V. natriegens* Bac5(1–17)-70S ribosome complexes for structural analysis.

Cryo-EM structure of the *V. natriegens* 70S ribosome

To generate *V. natriegens* Bac5(1–17)-70S ribosome complex, reconstituted *V. natriegens* 70S ribosomes were incubated with 100 μM Bac5(1–17) PrAMP and 100 μM spectinomycin (to reduce rotational heterogeneity), applied to cryo-grids and subjected to single particle cryo-EM analysis. From 3878 movie stacks, 405 140 particles were selected from 2D classes for refinement and subsequent 3D classification (Supplementary Fig. S1). As expected, the majority of particles contained vacant 70S ribosomes, however, despite the presence of spectinomycin, we observed multiple classes with differing degrees of 30S subunit rotation (Supplementary Fig. S1). From these, three classes were pooled and refined, yielding a final cryo-EM structure of the *V. natriegens* 70S ribosome with an average resolution of 2.8 Å (Supplementary Fig. S2). While the 50S subunit was well-resolved, with local resolution reaching towards 2.5 Å in the core, the density for the

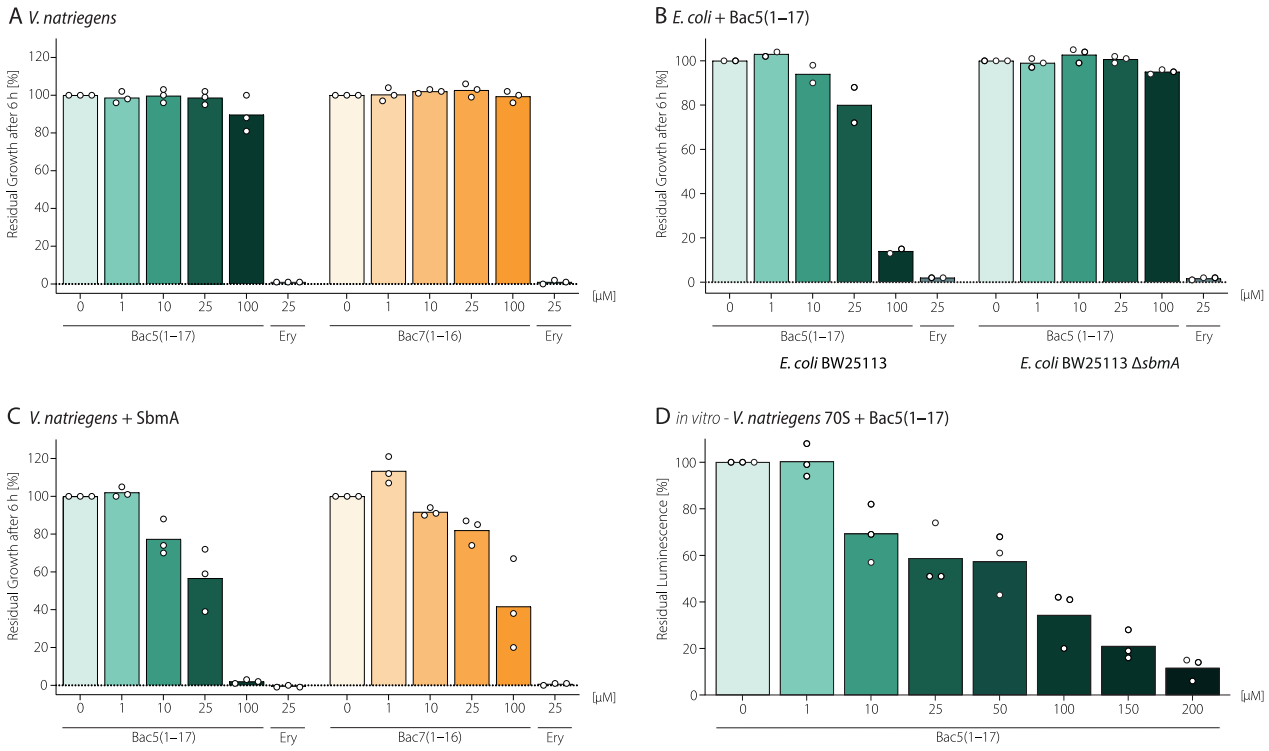

Figure 2. Growth assays and inhibition of translation by Bac5(1–17) and Bac7(1–16). (**A**) Growth assay showing the residual growth of wildtype *V. natriegens* (lacking SbmA, pAL0167_ColE1_sfGFP) after 6 h at 37°C when incubated with 0, 1, 10, 25, or 100 μM of Bac5(1–17) (green bars) or Bac7(1–16) (yellow bars), or 25 μM of the positive control antibiotic erythromycin (Ery). (**B**) Growth assay showing the residual growth of *E. coli* wildtype strain BW251113 (left) or BW25113 Δ*sbmA* (right) after 6 h at 37°C when incubated with 0, 1, 10, 25, or 100 μM of Bac5(1–17) (green bars), or 25 μM of the positive control antibiotic erythromycin (Ery). (**C**) Growth assay showing the residual growth of *V. natriegens* expressing heterologous SbmA (+SbmA, pAL0155_ColE1_SbmA) after 6 h at 37°C when incubated with 0, 1, 10, 25, or 100 μM of Bac5(1–17) (green bars) or Bac7(1–16) (yellow bars), or 25 μM of the positive control antibiotic erythromycin (Ery). For panels (A)–(C), all experiments were performed in triplicate ($n = 3$) and the bars represent the mean. (**D**) *In vitro* translation of firefly luciferase on *V. natriegens* ribosomes in the presence of increasing concentrations of Bac5(1–17). The luminescence in the absence of Bac5(1–17) was normalized as 100% and all bars represent the normalized mean of triplicate experiments ($n = 3$). Each replica is individually plotted as a white dot.

30S subunit was poorly resolved due to averaging of different rotational states (Supplementary Fig. S2). Therefore, focused refinement was performed with partial particle subtraction using masks around the 30S and 50S subunits, yielding final reconstructions of the *V. natriegens* 30S and 50S subunits at 2.8 and 2.7 Å resolution, respectively (Fig. 3A–D and (Supplementary Figs S1 and S2). For the 30S subunit, the body was well-resolved, with local resolution reaching towards 2.5 Å, whereas the head was less resolved, especially at the periphery (Supplementary Fig. S2), most likely due to independent head-swivel relative to the body. Overall, the architecture of the *V. natriegens* 70S ribosome (Fig. 3A–D) is highly homologous with the *E. coli* 70S ribosome, consistent with relatively close phylogenetic relationship.

As expected, additional density was observed for spectinomycin bound to the neck region of the 30S subunit (Fig. 3E). Spectinomycin interacts with 16S rRNA nucleotides located within h34, encompassing direct hydrogen bonds with A1202-G1204, C1073-G1074, C1076, and G1078 (Fig. 3E). These interactions are, within the resolution limits, identical to those observed for spectinomycin bound to the *E. coli* or *Enterococcus faecalis* 70S ribosome (Supplementary Fig. S3) [42, 50], which is not unexpected since all 16S rRNA nucleotides observed within the spectinomycin binding site are conserved between the three organisms. We also observe two water-mediated interactions between spectinomycin and the 16S rRNA that were reported in the *E. coli* 70S ribosome, namely, with A1077 (*Ec*A1067) and C1079 (*Ec*C1069) [42]. In addition, we observe two previously unreported water-mediated interactions from aminocyclitol ring of spectinomycin with U1080 and G1204 (Fig. 3E). The aminocyclitol ring of spectinomycin comes into close proximity (4–5 Å) of a loop within ribosomal protein uS5, which is located on the body, and therefore water-mediated interactions with this moiety may depend on the functional and rotational state of the ribosome.

Following modeling of the components of the 50S subunit (Fig. 3C and D), additional density remained within the ribosomal exit tunnel that we could unambiguously attribute to Bac5(1–17) (Fig. 3F). The high local resolution (2.5 Å) and excellent quality of the cryo-EM density for Bac5(1–17) enabled a *de novo* model for the complete peptide to be generated, including accurate placement of most sidechains. The exceptions were the terminal residues, Arg1 at the N-terminus and Tyr16-Pro17 at the C-terminus, which were poorly resolved (Fig. 3F) and density was only observed at lower thresholds (Supplementary Fig. S2). Additional density that we assigned to 12 water molecules was also observed mediating interactions between the Bac5(1–17) peptide and components of the ribosomal exit tunnel (Fig. 3F). Overall, the orientation of the

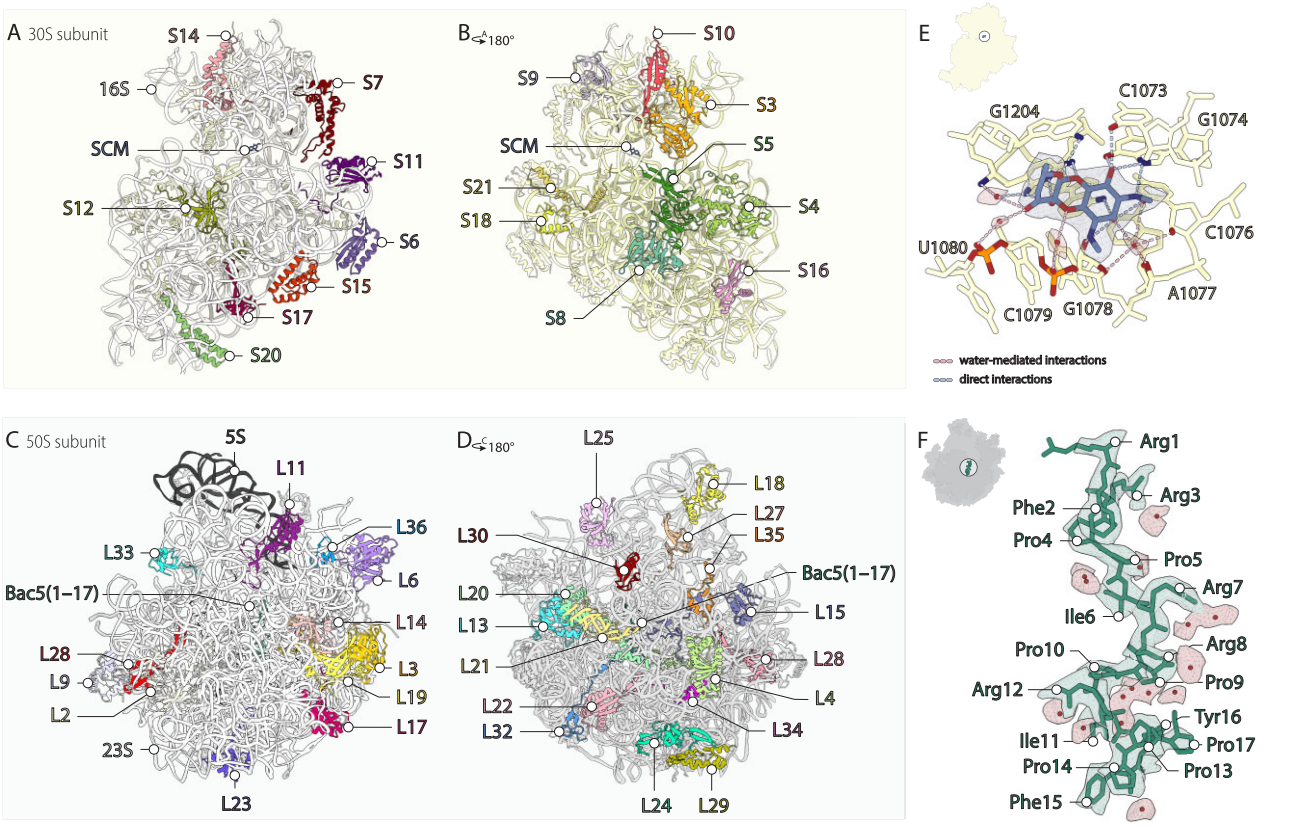

Figure 3. Cryo-EM structure of the *V. natriegens* Bac5-50S and SCM-30S complex. (**A**, **B**) Molecular model of the 30S ribosomal subunit with the individual ribosomal proteins and the 16S rRNA highlighted. The second view of the 30S is rotated 180° around the y axis. (**C**, **D**) Molecular model of the 50S ribosomal subunit with the individual ribosomal proteins, 5S and 23S rRNA highlighted. The 50S is shown in the crown view; the second panel shows this view rotated by 180°. (**E**) Isolated cryo-EM density map (mesh) with the molecular model of spectinomycin (SCM) and surrounding water molecules (spheres). The 16S nucleotide labels follow *V. natriegens* numbering, and interacting atoms are color-coded by element. SCM binds between the head and body of the 30S subunit. Dashed light blue lines indicate potential hydrogen bonds, while rose-colored dashed lines represent water-mediated interactions. (**F**) Isolated cryo-EM map density (mesh) of Bac5(1–17) and waters with the respective molecular models. Bac5(1–17) binds with its N-terminus in the PTC, while the C-terminus extends deeper into the polypeptide tunnel.

Bac5(1–17) was such that the N-terminal residues were located at the PTC and the C-terminal residues were oriented down the tunnel towards the constriction (Fig. 3F), i.e. opposite to that of a nascent polypeptide as it is being synthesized.

Interaction of Bac5(1–17) with the ribosomal exit tunnel

Interaction of Bac5(1–17) utilizes a combination of direct and water-mediated hydrogen bonding as well as stacking interactions between the peptide and 23S rRNA nucleotides of the 50S subunit (Fig. 4A–G and Supplementary Fig. S4). Interaction of the N-terminal half of the peptide is predominantly with 23S rRNA nucleotides located at the PTC and appears to be driven predominantly by hydrogen bond interactions that utilize the backbone nitrogen and carbonyl-oxygens of residues Arg1, Arg3, Ile6, Arg7, and Arg8 of Bac5(1–17) (Fig. 4A). The short distances (2.6–2.7 Å) between the donors and acceptors suggest the presence of strong hydrogen bond interactions. In addition, direct hydrogen bonds are formed between Arg7 and Arg8 with G2047 and G2491, respectively (Fig. 4B) and one stacking interaction between Arg8 and A2048 (EcA2062) (Fig. 4C). The N-terminal region of Bac5(1–17) is further stabilized by water-mediated interactions that link the carbonyl-oxygens of Pro4 and Pro5 of Bac5(1–17) with U2570 (EcU2584), and the backbone nitrogen of Ile6 with C2049 (EcC2063) (Fig. 4D). Additionally, we observe a water-mediated interaction between the backbone of Arg7 and two water molecules, bridging contacts to A2489 and G2491. Similarly, the side chain of Arg8 participates in a water-mediated network that connects Pro13, C2596 and C2597 (Fig. 4D). Collectively, these interactions are likely to be important since a Bac5 variant lacking the first four residues lost antimicrobial activity and was a poor inhibitor of *in vitro* translation assays [18]. In contrast to the N-terminus, interaction of the C-terminal half of Bac5(1–17) is centered on 23S rRNA nucleotides that comprise the exit tunnel, and utilizes predominantly stacking interactions between the sidechains of residues of Bac5(1–17) with the 23S rRNA nucleobases (Fig. 4E, F). Specifically, Pro9, Arg12, and Phe15 participate in stacking interactions with A2048 (EcA2062), U2595 (EcU2609) and C2596 (EcC2610), respectively (Fig. 4F). By contrast, only a single direct hydrogen bond between the side chain of Arg12 and C2596 (EcC2610) is evident. Regarding water-mediated hydrogen bonds, one water molecule mediates the interaction between the backbones of Pro9 and Ile11, thereby stabilizing the peptide intramolecularly. Furthermore, the backbones of Arg12 and Ile11 are associated with U2595 via two intervening water molecules (Fig. 4F-G and Supplementary Fig. S4). Mutagenesis studies indicate that the core of Bac5(1–17) encompassing residues Pro5–Phe15 is critical for antimicrobial activity

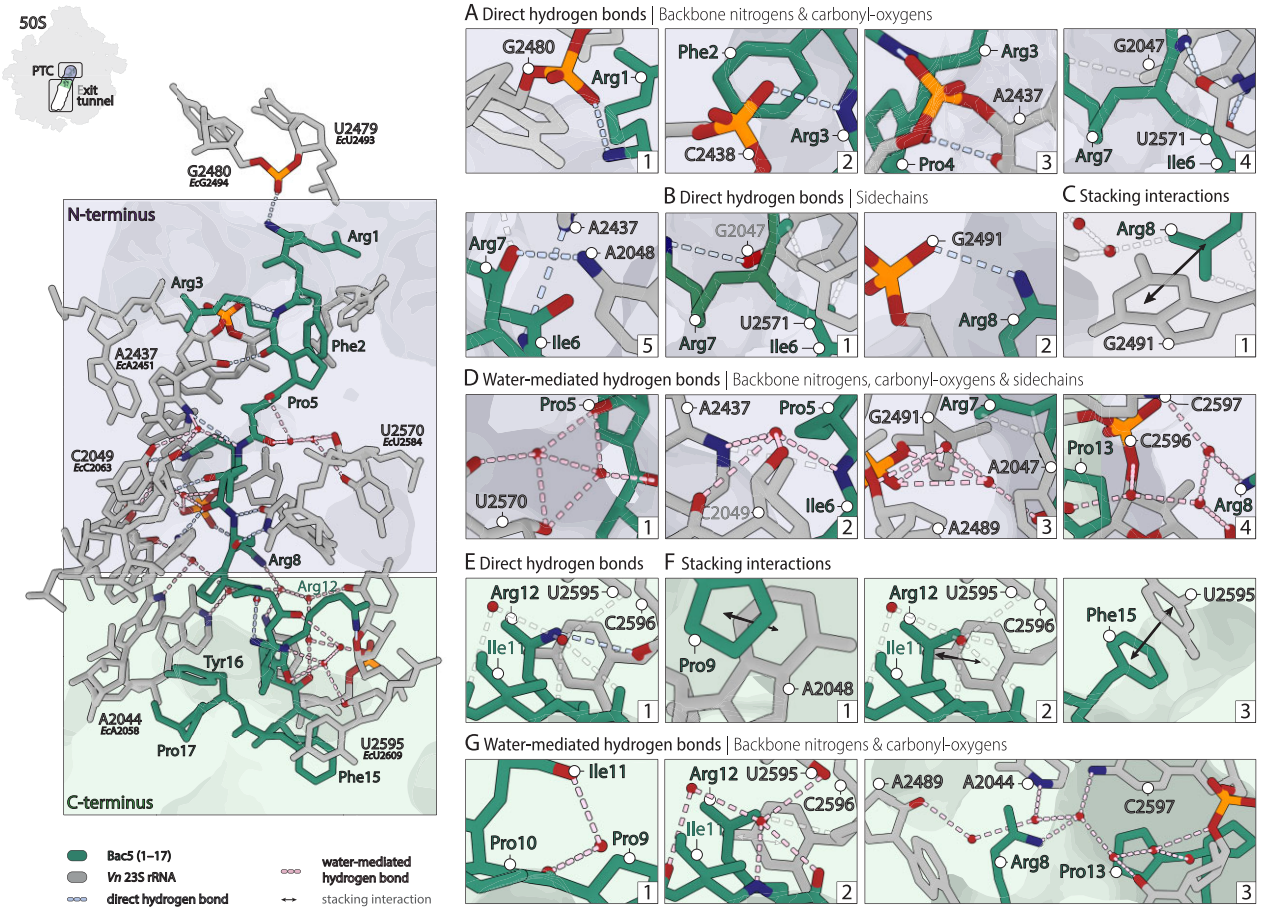

Figure 4. Interactions of Bac5(1–17) with nucleotides of the *V. natriegens* 50S subunit. Interactions between Bac5(1–17) and its binding site are highlighted with a purple background for residues from the N-terminal region and a light green background for those from the C-terminal region (**A**) Direct hydrogen bond interactions (blue dashed line) between the backbone nitrogen atoms and carbonyl oxygens of the N-terminal end of Bac5(1–17) and nucleotides of the 23S rRNA (A1–A5). (**B**) Direct hydrogen bond interactions involving N-terminal residues of Bac5(1–17) (B1–B2). (**C**) Stacking interactions (arrows) mediated by Arg8 in Bac5(1–17) (C1). (**D**) Water-mediated hydrogen bonds (dashed lines) of residues from the N-terminus (D1–D4). (**E**) Direct hydrogen bonds between C2596 towards the side chains of Arg12 from the C-terminal part of Bac5(1–17) (E1). (**F**) Stacking interactions of the C-terminal part of Bac5(1–17) (F1–F3). (**G**) Water-mediated hydrogen bonds between the backbone nitrogen atoms and carbonyl oxygens of the C-terminus (G1–G3).

since substitutions of these positions to Gly, Ala, Ser, Pro, Glu, or Phe generally increased the MIC of the peptide, whereas substitutions at the N- or C-terminus were tolerated better [19]. Reduction in inhibitory activity was also observed in *in vitro* translation assays when single central residues were mutated to alanines, whereas inhibitory activity was better tolerated when alanine mutations were introduced at the N- and C-termini [19]. Collectively, this data is consistent with the relatively poorly ordered N- and C-termini of the Bac5(1–17) observed in the Bac5(1–17)-70S structure.

Bac5(1–25) was shown previously to be less effective at inhibiting *in vitro* translation using *Thermus thermophilus* compared to that determined in *E. coli* [17]. Similar findings were also observed when comparing the inhibitory activity of Bac5(1–25) in a rabbit reticulocyte lysate-based assay [17]. We therefore aligned both *T. thermophilus* 70S ribosomes and *Oryctolagus cuniculus* (rabbit) 80S ribosomes to our Bac5(1–17)-70S structure and looked for differences in the Bac5(1–17) binding site (Supplementary Fig. S5). This analysis revealed a remarkable conservation in the Bac5(1–17) binding site between bacteria and eukaryotes and did not provide an obvious explanation for the reduced activity of Bac5 in the *T. thermophilus* and rabbit translation assays. Although some steric clashes were observed between Bac5(1–17) and rRNA nucleotides in the *T. thermophilus* 70S and *O. cuniculus* 80S ribosomes, the clashes were restricted to conserved nucleotides that are structurally flexible and adopt different conformations in ribosomes depending on the functional state, for example, A2062 (*Oc*A3908) and U2585 (*Tt*U2595) (Supplementary Fig. S5). Moreover, we observe similar clashes when comparing with the *E. coli* 70S ribosome, where Bac5 displays potent inhibitory activity using *in vitro* translation assays [17–19]. Therefore, we do not believe that these clashes are the reason for the differences in activity of Bac5, but rather speculate that the longer Bac5 derivatives, such as Bac5(1–25) and Bac5(1–31), can reach deeper into the tunnel and interact with the less-conserved ribosomal proteins uL4 and uL22, which are more likely to contribute to species-specific differences in Bac5 activity.

We also believe that the binding site determined here for the bovine Bac5(1–17) is likely to be identical for that of Bac5(1–17) from other mammals, such as sheep and goats, since the sequence is highly conserved. Within the first 17 amino acids, the only difference is at position 16, where bovine Bac5(1–

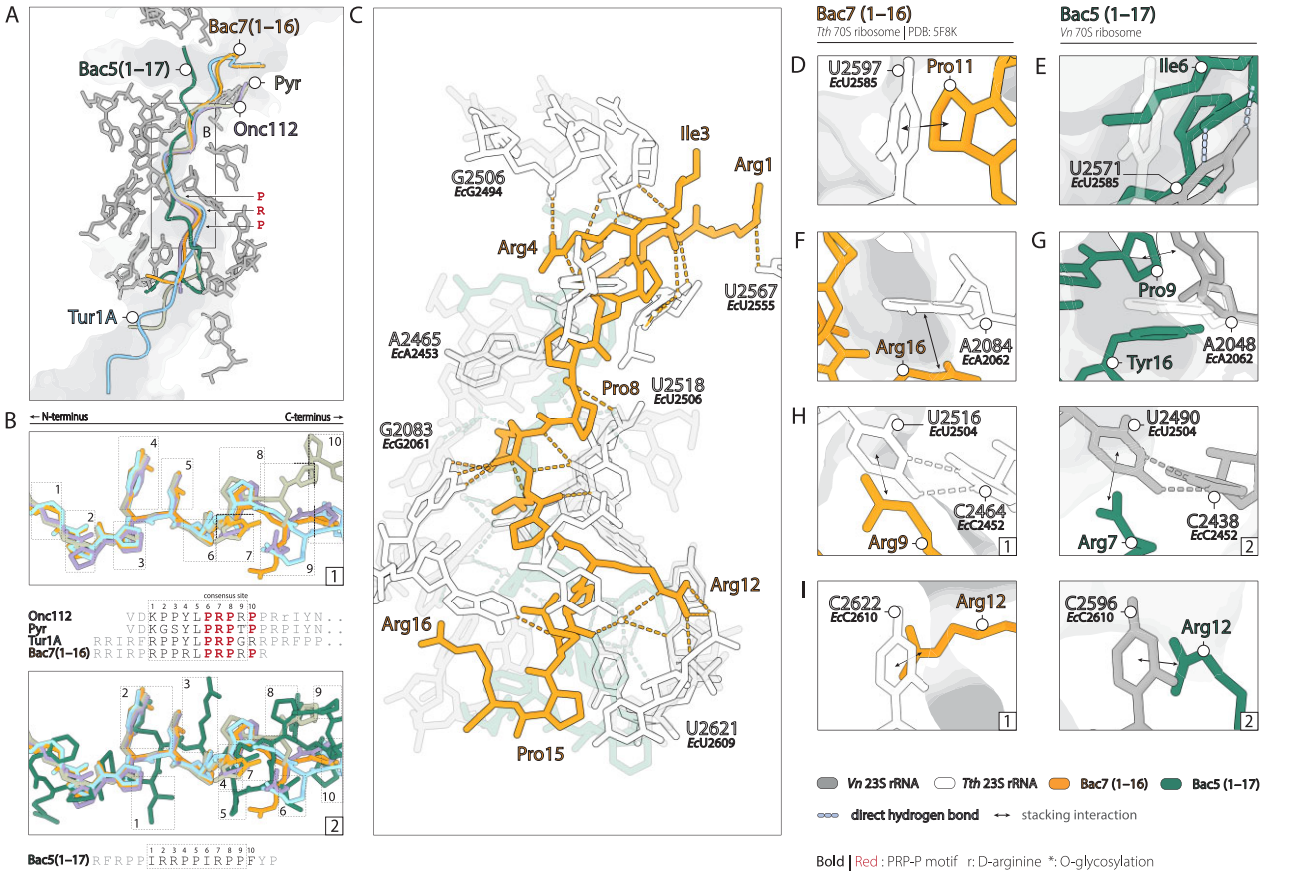

Figure 5. Comparison of the binding modes of Bac5(1–17) and other type I PrAMPs, such as Bac7(1–16). (**A**) Overlay of Type I PrAMPs, including Bac7(1–16) [8], Pyr [8], Onc112 [6], and Tur1A [10], with the structure of Bac5 (1–17). (**B**) The top panel (B1) highlights a close-up of the consensus sequence of PrAMPs from (**A**), with residues numbered 1–9 and the aligned sequences shown below. The consensus sequence is outlined with dashed lines, while the conserved PRP-P motif is marked in bold. The lower panel (B2) displays the same overlay, now focusing on Bac5(1–17), with its corresponding sequence alignment shown below. (**C**) Comparison of the binding sites of Bac7(1–16) and Bac5(1–17) within ribosomes from *T. thermophilus* and *V. natriegens*, respectively. (**D**) Pro11 of Bac7 forms a stacking interaction with U2597 (equivalent to *Ec*U2585) in the 23S rRNA of *T. thermophilus*. (**E**) The corresponding nucleotide in *V. natriegens* U2571 (*Ec*U2585) adopts a different conformation. (**F**) In *T. thermophilus*, A2084 (*Ec*A2062) extends into the tunnel lumen, stacking with Arg16 of Bac7. (**G**) In *V. natriegens*, the corresponding nucleotide (A2048) lies flat against the tunnel wall, stacking with Pro9 of Bac5. (**H**) Arg9 of Bac7(1–16) stacks with U2516 (*Ec*U2504), a similar interaction to Bac5(1–17), where Arg7 stacks with U2490 (*Ec*U2504). (**I**) Both Bac5(1–17) and Bac7(1–16) exhibit a conserved stacking interaction via Arg12 with *Ec*C2610, differing only in the positioning of their side chains.

17) contains Tyr, whereas sheep and goat Bac5(1–17) contain Arg and Asn, respectively. Although Tyr16 is not resolved in our structure, we note that the natural Bac5 sequence is 43 amino acids long and, therefore, the C-terminal region in the Bac5(1–17) may be better resolved in the context of a longer peptide. Indeed, the antimicrobial activity against *E. coli* as well as the inhibitory activity using *in vitro* translation assays of bovine Bac5(1–25) was identical to that observed for the sheep and goat Bac5(1–25) [17].

Unique binding mode of Bac5(1–17) compared to Bac7 and other type I PrAMPs

The orientation of Bac5(1–17) within the exit tunnel, i.e. with the N-terminus located at the PTC and the C-terminus directed towards the tunnel constriction, is the same as observed previously for other type I PrAMPs, such as Bac7, Onc112, metalnikowin I, pyrrhocoricin, Tur1A, and more recently for rumidicin-2 (Fig. 5A) [5–11]. Comparison of these PrAMPs reveals that despite the divergence at the N- and C-termini, the core region of the PrAMPs adopts a very similar conformation on the ribosome, consistent with the sequence conservation, including a conserved PRP motif (Fig. 5A and B). By contrast, Bac5(1–17) adopts a distinct conformation within the exit tunnel when compared to other type I PrAMPs, including the core region of Bac5(1–17), which does not contain a single PRP motif (Fig. 5B). As expected, the binding mode of Bac5(1–17) is also completely distinct from type II PrAMPs, such as apidaecin and drosocin [12–14, 16, 51, 52] (Supplementary Fig. S6).

Comparison of the ribosome structures of Bac5(1–17) with Bac7(1–16) illustrates the high degree of divergence in terms of the interactions with the components of the ribosomal exit tunnel (Fig. 5C). For example, in the Bac7(1–16) structure Pro11 of Bac7 stacks upon EcU2585 within the PTC. By contrast, in the Bac5(1–17) structure, Ile6 of Bac5 sterically clashes with the position of EcU2585 in the Bac7 structure, leading EcU2585 to adopt a different conformation which is stabilized by direct hydrogen bonds with the backbone of Bac5 (Fig. 5D and E). Similarly, in the Bac7(1–16) structure, EcA2062 adopts a rotated conformation such that the base extends into the tunnel lumen, where it is stacked upon by

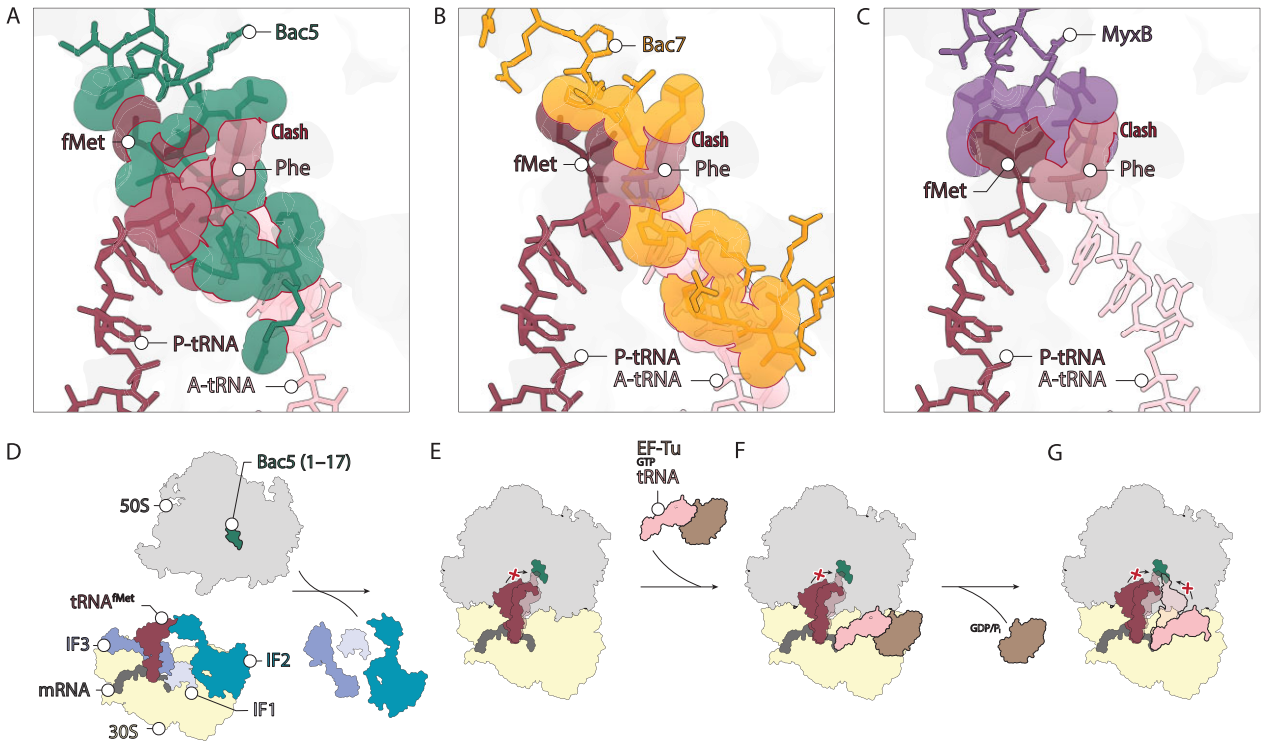

Figure 6. Model for the inhibition mechanism of Bac5(1–17). (**A**) The N-terminal region of Bac5(1–17) (teal green) causes steric problems with both the aminoacylated fMet-tRNA (dark red) in the P-site and the aminoacylated Phe-tRNA in the A-site (pale pink) [54], highlighted by red lines indicating the clashing atoms. (**B**) When aligned with Bac7(1–16) [8], similar steric interactions can be observed with the P- and A-site tRNAs. However, the clash with the A-site tRNA is more extensive compared to the one caused by Bac5(1–17). (**C**) Myxovalargin B (MyxB, purple) [53] also induces steric clashes with tRNAs in both the P- and A-sites, primarily due to interactions with the amino acids of the tRNAs. (**D**–**G**) Based on structural alignments with tRNAs, a potential mechanism for Bac5-mediated translation inhibition is proposed. Bac5 binds to the 50S ribosomal subunit prior to the assembly of the 70S translating ribosome (D). This binding likely hinders translation initiation by disrupting the proper positioning of fMet-tRNA in the P-site (E). Additionally, the placement of the A-site tRNA by EF-Tu is blocked due to steric interference between Bac5 and both the amino acid and the CCA-end of the A-site tRNA (F-G). The illustration of the mechanism was inspired by [2].

the sidechain of Arg16 of Bac7. By contrast, EcA2062 lies flat against the exit tunnel in the presence of Bac5(1–17) and is stacked upon by Pro9 of Bac5(1–17) (Fig. 5F and G). Nevertheless, despite the overall differences in the interactions, a few similarities in terms of stacking interactions are observed, for example, both Bac5 and Bac7 form stacking interactions with the C2452 = U2504 base-pair, namely, using the sidechains of Arg7 and Arg9, respectively (Fig. 5H), and the sidechain of Arg12 of both Bac5 and Bac7 forms stacking interactions with the nucleobase of EcC2610 (Fig. 5I).

Bac5(1–17) overlaps A- and P-site tRNAs at the PTC

Based on toeprinting assays, Bac5 fragments have been proposed to interfere with the accommodation of the first aminoacyl-tRNA at the A-site of the PTC, and thereby preventing translation elongation [17], consistent with the type I mechanism of action described for the related PrAMP, Bac7 [8, 9]. Therefore, we superimposed a bacterial ribosome structure containing an accommodated Phe-tRNA at the A-site of the PTC with the binding position of Bac5, revealing that indeed the N-terminal region of Bac5 overlaps with the CCA-end of the A-site tRNA (Fig. 6A). In particular, we observe that residues Arg1-Pro4 would sterically clash with the C75 and A76 of the A-tRNA and residues Pro5-Ile6 of Bac5 with the phenylalanine moiety (Fig. 6A). The extent of overlap is less than that observed for Bac7, where the N-terminal residues Arg1-Ile3 penetrate deeper into the A-tRNA binding site (Fig. 6B). However, unlike Bac7(1–16) that exhibits only modest overlap with the initiator tRNA in the P-site (Fig. 6B), the binding position of Bac5(1–17) clashes more extensively with the terminal A76 and especially the fMet moiety of the initiator tRNA (Fig. 6A). This clash is even more extensive than that observed for the myxobacterial antibiotic myxovalargin (Fig. 6C), where accommodation of the initiator tRNA at the P-site was also shown to be prevented [53]. Thus, we propose that unlike most type I PrAMPs, Bac5 is likely to not only interfere with accommodation of the aminoacyl-tRNA at the A-site during elongation, but also the fine placement of the initiator tRNA at the P-site during translation initiation.

Discussion

Collectively, our structure of Bac5(1–17) in complex with the *V. natriegens* ribosome, together with previous biochemical studies [11, 17–19], enables us to present a model for the mechanism of action of Bac5(1–17). Like other type I PrAMPs, Bac5(1–17) binds within the exit tunnel of the large 50S subunit, and, therefore, can in principle interact with its binding site on the vacant 50S subunit prior to translation initiation (Fig. 6D). Previous biochemical studies using toeprinting assays indicate that, in the presence of Bac5, ribosomes can

adopt an initiation state with the initiator fMet-tRNA bound at the P-site of the small subunit of ribosome (Fig. 6E and F). However, given that the binding site of Bac5 overlaps sterically with the A76 and fMet moiety of the initiator tRNA, we suggest that the initiator tRNA cannot accommodate at the P-site at the PTC of the large subunit (Fig. 6E and F). The extent of overlap is more extensive than observed for other type I PrAMPs (Fig. 6A), although we note that careful comparison also reveals steric clashes for type I PrAMPs, such as Bac7 (Fig. 6B) [2, 3, 5–11], suggesting that this mechanism may also be conserved. Additionally, the N-terminal residues of Bac5 also sterically overlap with the CCA-end of an aminoacylated-tRNA accommodated at the A-site of the PTC (Fig. 6A), as observed for other type I PrAMPs, such as Bac7 (Fig. 6B) [2, 3, 5–11]. Thus, Bac5 is likely to exhibit a dual inhibitory mechanism to interfere with accommodation of both the initiator fMet-tRNA at the P-site and the aminoacylated-tRNA at the A-site of the PTC (Fig. 6G). We acknowledge that in such a scenario inhibition of the initiator tRNA may be the dominant step, however, this needs to be investigated further. As mentioned above, such a mechanism of action is reminiscent of the unrelated myxobacterial nonribosomal peptide antibiotic myxovalargin (Fig. 6C) [53]. The mode of action on the ribosome of Bac5 is likely to be identical for the wildtype bovine Bac5 PrAMP, as well as Bac5 PrAMPs from other species, such as sheep and goat Bac5, which have a high sequence similarity with bovine Bac5 [19].

Perhaps the most striking finding from our study is that although Bac5 binds within the exit tunnel of the ribosome with the same orientation as other type I PrAMPs, and also inhibits translation using a similar mechanism of action, we observe a completely distinct mode of binding and interaction of Bac5 with the ribosome compared to other PrAMPs. To date, the central region of type I PrAMPs contain a conserved PRP motif that adopts a similar conformation and mode of interaction with ribosomal tunnel (Fig. 5A and B). By contrast, Bac5 does not contain a single PRP motif and therefore the central region of Bac5 establishes a distinct conformation and unrelated mode of interaction with the ribosome (Fig. 5). For this reason, we propose to refer to PRP-containing type I PrAMPs, such as Bac7, as type Ia PrAMPs, and non-PRP-containing type I PrAMPs, such as Bac5, as type Ib PrAMPs. It will be interesting in the future to see whether other type I PrAMPs exist that exhibit distinct binding modes and mechanisms of action to the type Ia and Ib PrAMPs defined in this study. Lastly, we hope that the structure of the *V. natriegens* 70S ribosome will provide a reference structure for future endeavours using *V. natriegens* as a model system for molecular biology or biotechnological applications.

Acknowledgements

We would like to thank Jiří Nováček for data collection, the iNEXT-Discovery and the cryo-electron microscopy and tomography core facility CEITEC MU of CIISB. We also thank rotation students Irene Protschky and Lev Böttger for help with the biochemical assays and Max Berger for assisting with final model refinements.

Author contributions: K.R. and M.Mo. performed all *in vivo* and *in vitro* assays, respectively. M.Ma. and A.L provided reagents. T.O.K. and B.B. performed the cryo-EM analysis. K.R. and T.O.K. generated all figures. D.N.W., G.B., and M.S. supervised the project. All authors analyzed the data and contributed to helping K.R. and D.N.W. in writing the paper.

Supplementary data

Supplementary data is available at NAR online.

Conflict of interest

None declared.

Funding

This work was supported by the Deutsche Forschungsgemeinschaft (DFG) [SPP 1879 to D.N.W. and G.B.], the iNEXT-Discovery funded by the Horizon 2020 program of the European Commission and the cryo-electron microscopy and tomography core facility CEITEC MU of CIISB, Instruct-CZ Centre supported by MEYS CR (LM2018127). Funding to pay the Open Access publication charges for this article was provided by University of Hamburg.

Data availability

Cryo-EM maps of the *V. natriegens* 70S ribosome in complex with Bac5(1–17) have been deposited in the Electron Microscopy Data Bank (EMDB) with accession codes EMD-51946 [https://www.ebi.ac.uk/pdbe/entry/emdb/EMD-51946] (30S subunit) and EMD-51947 [https://www.ebi.ac.uk/pdbe/entry/emdb/EMD-19638] (50S subunit) and the associated molecular models for the *V. natriegens* 30S with spectinomycin and the 50S subunit with Bac5(1–17) have been deposited in the Protein Data Bank with accession codes 9H90 [https://doi.org/10.2210/pdb9h90] and 9H91 [https://doi.org/10.2210/pdb9h91/pdb], respectively.

References

1. Scocchi M, Tossi A, Gennaro R. Proline-rich antimicrobial peptides: converging to a non-lytic mechanism of action. *Cell Mol Life Sci* 2011;**68**:2317–30. https://doi.org/10.1007/s00018-011-0721-7
2. Graf M, Mardirossian M, Nguyen F *et al.* Proline-rich antimicrobial peptides targeting protein synthesis. *Nat Prod Rep* 2017;**34**:702–11. https://doi.org/10.1039/C7NP00020K
3. Graf M, Wilson DN. Intracellular antimicrobial peptides targeting the protein synthesis machinery. *Adv Exp Med Biol* 2019;**1117**:73–89. https://doi.org/10.1007/978-981-13-3588-4_6
4. Sola R, Mardirossian M, Beckert B *et al.* Characterization of cetacean proline-rich antimicrobial peptides displaying activity against ESKAPE pathogens. *Int J Mol Sci* 2020;**21**:7367. https://doi.org/10.3390/ijms21197367
5. Panteleev PV, Pichkur EB, Kruglikov RN *et al.* Rumicidins are a family of mammalian host-defense peptides plugging the 70S ribosome exit tunnel. *Nat Commun* 2024;**15**:8925. https://doi.org/10.1038/s41467-024-53309-y
6. Seefeldt AC, Nguyen F, Antunes S *et al.* The proline-rich antimicrobial peptide Onc112 inhibits translation by blocking and destabilizing the initiation complex. *Nat Struct Mol Biol* 2015;**22**:470–5. https://doi.org/10.1038/nsmb.3034
7. Roy RN, Lomakin IB, Gagnon MG *et al.* The mechanism of inhibition of protein synthesis by the proline-rich peptide oncocin. *Nat Struct Mol Biol* 2015;**22**:466–9. https://doi.org/10.1038/nsmb.3031

8. Seefeldt AC, Graf M, Perebaskine N *et al.* Structure of the mammalian antimicrobial peptide Bac7 (1-16) bound within the exit tunnel of a bacterial ribosome. *Nucleic Acids Res* 2016;**44**:2429–38. https://doi.org/10.1093/nar/gkv1545
9. Gagnon MG, Roy RN, Lomakin IB *et al.* Structures of proline-rich peptides bound to the ribosome reveal a common mechanism of protein synthesis inhibition. *Nucleic Acids Res* 2016;**44**:2439–50. https://doi.org/10.1093/nar/gkw018
10. Mardirossian M, Perebaskine N, Benincasa M *et al.* The dolphin proline-rich antimicrobial peptide Tur1A inhibits protein synthesis by targeting the bacterial ribosome. *Cell Chemical Biology* 2018;**25**:530–9. https://doi.org/10.1016/j.chembiol.2018.02.004
11. Mardirossian M, Sola R, Beckert B *et al.* Peptide inhibitors of bacterial protein synthesis with broad spectrum and SbmA-independent bactericidal activity against clinical pathogens. *J Med Chem* 2020;**63**:9590–602. https://doi.org/10.1021/acs.jmedchem.0c00665
12. Florin T, Maracci C, Graf M *et al.* An antimicrobial peptide that inhibits translation by trapping release factors on the ribosome. *Nat Struct Mol Biol* 2017;**24**:752–7. https://doi.org/10.1038/nsmb.3439
13. Graf M, Huter P, Maracci C *et al.* Visualization of translation termination intermediates trapped by the Apidaecin 137 peptide during RF3-mediated recycling of RF1. *Nat Commun* 2018;**9**:3053. https://doi.org/10.1038/s41467-018-05465-1
14. Chan KH, Petrychenko V, Mueller C *et al.* Mechanism of ribosome rescue by alternative ribosome-rescue factor B. *Nat Commun* 2020;**11**:4106. https://doi.org/10.1038/s41467-020-17853-7
15. Koller TO, Morici M, Berger M *et al.* Structural basis for translation inhibition by the glycosylated drosocin peptide. *Nat Chem Biol* 2023;**19**:1072–81. https://doi.org/10.1038/s41589-023-01293-7
16. Lauer SM, Reepmeyer M, Berendes O *et al.* Multimodal binding and inhibition of bacterial ribosomes by the antimicrobial peptides Api137 and Api88. *Nat Commun* 2024;**15**:3945. https://doi.org/10.1038/s41467-024-48027-4
17. Mardirossian M, Barriere Q, Timchenko T *et al.* Fragments of the nonlytic proline-rich antimicrobial peptide Bac5 kill *Escherichia coli* cells by inhibiting protein synthesis. *Antimicrob Agents Chemother* 2018;**62**:e00534-18. https://doi.org/10.1128/AAC.00534-18
18. Mardirossian M, Sola R, Degasperi M *et al.* Search for shorter portions of the proline-rich antimicrobial peptide fragment Bac5 (1-25) that retain antimicrobial activity by blocking protein synthesis. *ChemMedChem* 2019;**14**:343–8. https://doi.org/10.1002/cmdc.201800734
19. Mardirossian M, Sola R, Beckert B *et al.* Proline-rich peptides with improved antimicrobial activity against *E. coli*, *K. pneumoniae*, and *A. baumannii*. *ChemMedChem* 2019;**14**:2025–33. https://doi.org/10.1002/cmdc.201900465
20. Tokunaga Y, Niidome T, Hatakeyama T *et al.* Antibacterial activity of bactenecin 5 fragments and their interaction with phospholipid membranes. *J Pept Sci* 2001;**7**:297–304. https://doi.org/10.1002/psc.317
21. Hoff J, Daniel B, Stukenberg D *et al.* *Vibrio natriegens*: an ultrafast-growing marine bacterium as emerging synthetic biology chassis. *Environ Microbiol* 2020;**22**:4394–408. https://doi.org/10.1111/1462-2920.15128
22. Payne WJ. Studies on bacterial utilization of uronic acids. III. Induction of oxidative enzymes in a marine isolate. *J Bacteriol* 1958;**76**:301–7. https://doi.org/10.1128/jb.76.3.301-307.1958
23. Weinstock MT, Hesek ED, Wilson CM *et al.* *Vibrio natriegens* as a fast-growing host for molecular biology. *Nat Methods* 2016;**13**:849–51. https://doi.org/10.1038/nmeth.3970
24. Eagon RG. *Pseudomonas natriegens*, a marine bacterium with a generation time of less than 10 minutes. *J Bacteriol* 1962;**83**:736–7. https://doi.org/10.1128/jb.83.4.736-737.1962
25. Hoffart E, Grenz S, Lange J *et al.* High substrate uptake rates empower *Vibrio natriegens* as production host for industrial biotechnology. *Appl Environ Microb* 2017;**83**:e01614-17. https://doi.org/10.1128/AEM.01614-17
26. Tschirhart T, Shukla V, Kelly EE *et al.* Synthetic biology tools for the fast-growing marine bacterium *Vibrio natriegens*. *ACS Synth Biol* 2019;**8**:2069–79. https://doi.org/10.1021/acssynbio.9b00176
27. Lee HH, Ostrov N, Wong BG *et al.* Functional genomics of the rapidly replicating bacterium *Vibrio natriegens* by CRISPRi. *Nat Microbiol* 2019;**4**:1105–13. https://doi.org/10.1038/s41564-019-0423-8
28. Baba T, Ara T, Hasegawa M *et al.* Construction of *Escherichia coli K-12* in-frame, single-gene knockout mutants: the Keio collection. *Mol Syst Biol* 2006;**2**:2006.0008. https://doi.org/10.1038/msb4100050
29. Stukenberg D, Hensel T, Hoff J *et al.* The Marburg Collection: a Golden Gate DNA assembly framework for synthetic biology applications in *Vibrio natriegens*. *ACS Synth Biol* 2021;**10**:1904–19. https://doi.org/10.1021/acssynbio.1c00126
30. Blaha G, Stelzl U, Spahn CMT *et al.* Preparation of functional ribosomal complexes and the effect of buffer conditions on tRNA positions observed by cryoelectron microscopy. *Methods Enzymol* 2000;**317**:292–309. https://doi.org/10.1016/S0076-6879(00)17021-1
31. Kimanius D, Dong L, Sharov G *et al.* New tools for automated cryo-EM single-particle analysis in RELION-4.0. *Biochem J* 2021;**478**:4169–85. https://doi.org/10.1042/BCJ20210708
32. Zheng SQ, Palovcak E, Armache JP *et al.* MotionCor2: anisotropic correction of beam-induced motion for improved cryo-electron microscopy. *Nat Methods* 2017;**14**:331–2. https://doi.org/10.1038/nmeth.4193
33. Wagner T, Merino F, Stabrin M *et al.* SPHIRE-crYOLO is a fast and accurate fully automated particle picker for cryo-EM. *Commun Biol* 2019;**2**:218. https://doi.org/10.1038/s42003-019-0437-z
34. Beckert B, Leroy EC, Sothiselvam S *et al.* Structural and mechanistic basis for translation inhibition by macrolide and ketolide antibiotics. *Nat Commun* 2021;**12**:4466. https://doi.org/10.1038/s41467-021-24674-9
35. Heymann JB. Guidelines for using Bsoft for high resolution reconstruction and validation of biomolecular structures from electron micrographs. *Protein Sci* 2018;**27**:159–71. https://doi.org/10.1002/pro.3293
36. Watson ZL, Ward FR, Meheust R *et al.* Structure of the bacterial ribosome at 2 A resolution. *eLife* 2020;**9**:e60482. https://doi.org/10.7554/eLife.60482
37. Pettersen EF, Goddard TD, Huang CC *et al.* UCSF ChimeraX: structure visualization for researchers, educators, and developers. *Protein Sci* 2021;**30**:70–82. https://doi.org/10.1002/pro.3943
38. Emsley P, Lohkamp B, Scott WG *et al.* Features and development of Coot. *Acta Crystallogr D Biol Crystallogr* 2010;**66**:486–501. https://doi.org/10.1107/S0907444910007493
39. Winn MD, Ballard CC, Cowtan KD *et al.* Overview of the CCP4 suite and current developments. *Acta Crystallogr D Biol Crystallogr* 2011;**67**:235–42. https://doi.org/10.1107/S0907444910045749
40. Jumper J, Evans R, Pritzel A *et al.* Highly accurate protein structure prediction with AlphaFold. *Nature* 2021;**596**:583–9. https://doi.org/10.1038/s41586-021-03819-2
41. Abramson J, Adler J, Dunger J *et al.* Accurate structure prediction of biomolecular interactions with AlphaFold 3. *Nature* 2024;**630**:493–500. https://doi.org/10.1038/s41586-024-07487-w
42. Paternoga H, Crowe-McAuliffe C, Bock LV *et al.* Structural conservation of antibiotic interaction with ribosomes. *Nat Struct Mol Biol* 2023;**30**:1380–92. https://doi.org/10.1038/s41594-023-01047-y
43. Long F, Nicholls RA, Emsley P *et al.* AceDRG: a stereochemical description generator for ligands. *Acta Crystallogr D Struct Biol* 2017;**73**:112–22. https://doi.org/10.1107/S2059798317000067
44. Vagin AA, Steiner RA, Lebedev AA *et al.* REFMAC5 dictionary: organization of prior chemical knowledge and guidelines for its

use. *Acta Crystallogr D Biol Crystallogr* 2004;**60**:2184–95. https://doi.org/10.1107/S0907444904023510
45. Yamashita K, Palmer CM, Burnley T *et al.* Cryo-EM single-particle structure refinement and map calculation using Servalcat. *Acta Crystallogr D Struct Biol* 2021;**77**:1282–91. https://doi.org/10.1107/S2059798321009475
46. Liebschner D, Afonine PV, Baker ML *et al.* Macromolecular structure determination using X-rays, neutrons and electrons: recent developments in Phenix. *Acta Crystallogr D Struct Biol* 2019;**75**:861–77. https://doi.org/10.1107/S2059798319011471
47. Mattiuzzo M, Bandiera A, Gennaro R *et al.* Role of the *Escherichia coli* SbmA in the antimicrobial activity of proline-rich peptides. *Mol Microbiol* 2007;**66**:151–63. https://doi.org/10.1111/j.1365-2958.2007.05903.x
48. Runti G, Benincasa M, Giuffrida G *et al.* The mechanism of killing by the proline-rich peptide Bac7 (1-35) against clinical strains of*Pseudomonas aeruginosa* differs from that against other gram-negative bacteria. *Antimicrob Agents Chemother* 2017;**61**:e01660-16. https://doi.org/10.1128/AAC.01660-16
49. Chiba S, Kanamori T, Ueda T *et al.* Recruitment of a species-specific translational arrest module to monitor different cellular processes. *Proc Natl Acad Sci USA* 2011;**108**:6073–8. https://doi.org/10.1073/pnas.1018343108
50. Crowe-McAuliffe C, Murina V, Turnbull KJ *et al.* Structural basis for PoxtA-mediated resistance to phenicol and oxazolidinone antibiotics. *Nat Commun* 2022;**13**:1860. https://doi.org/10.1038/s41467-022-29274-9
51. Koller TO, Turnbull KJ, Vaitkevicius K *et al.* Structural basis for HflXr-mediated antibiotic resistance in Listeria monocytogenes. *Nucleic Acids Res* 2022;**50**:11285–300. https://doi.org/10.1093/nar/gkac934
52. Huang W, Baliga C, Aleksandrova EV *et al.* Activity, structure, and diversity of type II proline-rich antimicrobial peptides from insects. *EMBO Rep* 2024; **24**:5194-5211. https://doi.org/10.1038/s44319-024-00277-5
53. Koller TO, Scheid U, Kosel T *et al.* The myxobacterial antibiotic myxovalargin: biosynthesis, structural revision, total synthesis, and molecular characterization of ribosomal inhibition. *J Am Chem Soc* 2023;**145**:851–63. https://doi.org/10.1021/jacs.2c08816
54. Polikanov YS, Steitz TA, Innis CA. A proton wire to couple aminoacyl-tRNA accommodation and peptide-bond formation on the ribosome. *Nat Struct Mol Biol* 2014;**21**:787–93. https://doi.org/10.1038/nsmb.2871

Received: December 13, 2024. **Revised:** March 27, 2025. **Editorial Decision:** April 5, 2025. **Accepted:** April 14, 2025